Liquid Crystalline Metal-Free Phthalocyanines Designed for Charge and Exciton Transport

Julien Tant,[†] Yves Henri Geerts,*[,†] Matthias Lehmann,[†] Vinciane De Cupere,[†] Gaël Zucchi,[†] Bo Wegge Laursen,[‡] Thomas Bjørnholm,[‡] Vincent Lemaur,[§] Valérie Marcq,[§] Anick Burquel,[§] Emmanuelle Hennebicq,[§] Fabrice Gardebien,[§] Pascal Viville,[§] David Beljonne,[§] Roberto Lazzaroni,[§] and Jérôme Cornil*[,§]

Laboratoire de Chimie des Polymères, Université Libre de Bruxelles, CP 206/1 Boulevard du Triomphe, B-1050 Bruxelles, Belgium, Service de Chimie des Matériaux Nouveaux, Université de Mons-Hainaut, 20 Place du Parc, B-7000 Mons, Belgium, Nano-Science Center, University of Copenhagen, Univeritetsparken 5, DK-2100 Copenhagen, Denmark

Received: August 24, 2005

A joint theoretical and experimental study of the electronic and structural properties of liquid crystalline metal-free phthalocyanines bearing a strong potential for charge and exciton transport has been performed. The synthesis of such compounds has been triggered by quantum chemical calculations showing that: (i) hole transport is favored in metal-free phthalocyanines by their extremely low reorganization energy (0.045 eV) and large electronic splittings; and (ii) the efficiency of energy transfer along the one-dimensional discotic stacks is weakly affected by rotational disorder due to the two-dimensional character of the molecules. We have synthesized two metal-free phthalocyanines with different branched aliphatic chains on the gram scale to allow for a full characterization of their solid-state properties. The two compounds self-organize in liquid crystalline mesophases, as evidenced by optical microscopy, differential scanning calorimetry, X-ray powder diffraction, and molecular dynamics simulations. They exhibit a columnar rectangular mesophase at room temperature and a columnar hexagonal mesophase at elevated temperature.

Introduction

Since their discovery in 1907,[1] phthalocyanines (Pcs) have found many industrial applications as dyes and pigments[2] due to their outstanding photo- and thermal stability combined with rather simple synthetic procedures.[3] Pcs have also been widely investigated as molecular conductors[4] and photoconductors.[5] In 1982, Piechocki and Simon reported the first Pc exhibiting a columnar liquid crystalline (LC) mesophase.[6] Since then, numerous examples of disk-shaped, peripherally substituted Pcs, self-organizing into columnar liquid crystalline mesophases, have been reported.[7] Such functional materials are of high interest for photovoltaic (PV) applications. Several reasons can be invoked: (i) LC Pcs have the tendency to spontaneously form single-domain thin films with homeotropic alignment;[8] (ii) columnar stacks of Pcs are known to exhibit high charge carrier mobility for organic materials, on the order of 0.2 $cm^2/V \cdot s$[9] and exciton diffusion length as large as several hundreds nanometers;[10] (iii) Pcs intensely absorb in the red region of the solar spectrum, in contrast to most organic conjugated materials used nowadays in solar cells;[3] and (iv) Pcs have a relatively low oxidation potential, making them good electron donors in photoinduced electron-transfer processes.[11] The interest of LC Pcs is further reinforced by the recent discovery that PV devices fabricated with discotic LC hexabenzocoronene derivatives reach an external quantum efficiency of 34% near 490 nm, without any specific alignment of liquid crystalline disklike molecules.[12] The full potential of discotic LC Pcs in PV diodes has not been demonstrated yet because several obstacles remain, among them the control of the miscibility, morphology, and homeotropic alignment of blends composed of donor and acceptor LC discotics. A first step is the synthesis of donor and acceptor LC discotics that homeotropically align in various conditions as neat compounds.

In this contribution, the basis of theoretical considerations on model systems explains why Pcs derivatives have a strong potential as charge and exciton carriers in organic-based devices. We then report the synthesis and characterization of new mesogenic phthalocyanine derivatives with properties tailored to be suitable for photovoltaic applications by ensuring simple device manufacturing and high yield of photocurrent generation. The criteria are the following: (i) The synthetic pathway must be straightforward, with good yields, to allow the synthesis of the materials on the g-scale. (ii) Pc derivatives have to be highly soluble in common organic solvents to allow solution processing, e.g., by spin-coating or ink-jet printing, on a wide range of thickness. (iii) The Pc mesogens must form a columnar LC phase with a clearing temperature below 200 °C to allow for the formation of homeotropically aligned single-domain thin films upon slow cooling from the isotropic melt. 200 °C is viewed as an upper limit to keep device fabrication compatible with the use of flexible plastic substrates.[13] (iv) The mesophase should persist down to room temperature without tendency to crystallization because crystal nucleation and growth occur randomly and turn single-domain LC films into multidomain films with grain boundaries that are detrimental to charge transport.[14] Other groups have previously reported LC Pcs with some of the desired features but never with the full set of properties required for solar cell applications.[15] Two LC metal-free Pcs will be fully characterized in this paper (Scheme 1);

* Corresponding authors. E-mail: ygeerts@ulb.ac.be (Y.H.G.), Jerome@averell.umh.ac.be (J.C.).
[†] Université Libre de Bruxelles.
[‡] University of Copenhagen.
[§] Université de Mons-Hainaut.

10.1021/jp054778o CCC: $30.25
Published on Web 10/08/2005

SCHEME 1: Chemical Structure of Mesogenic Four-Fold Substituted Phthalocyanines: H2Pc-O-(12,8)$_4$ 1a and H2Pc-O-(14,10)$_4$ H2Pc-O-(14,10)4 1b[a]

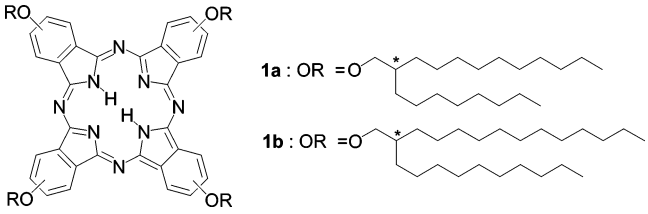

[a] Both compounds exist as a mixture of four isomers: D_{2h}:C_s:C_{2v}:C_{4h} with a statistical distribution 12.5:50:25:12.5, according to ref 16. (see Supporting Information). Alkoxy side chains have been used as racemates.

among them, the one with the longest side chains exhibits the required structural and physicochemical properties listed above.

Theoretical Considerations

The goal of this theoretical section is to demonstrate at a generic level the strong potential of phthalocyanines as charge and exciton carriers in organic-based devices by performing calculations on model stacks. The peripheral chains play an indirect role by defining the relative positions of the interacting conjugated cores and, hence, the amplitude of the molecular parameters involved in transport. They are, however, typically replaced by hydrogen atoms in the calculations of the electronic structure and photophysical properties, as exciton migration and charge transport are primarily governed by the π-conjugated core of the molecules.

Charge Transport. Charge migration in discotic liquid crystals generally occurs via a hopping mechanism because of the relatively high temperature range of the mesophase and the inherent disorder, which are two ingredients against a band model. In the hopping regime, the charges (holes or electrons) are localized over a single molecule and jump from disk to disk along the stack to yield a current. The rate of charge hopping k_{ET} can be estimated in first approximation by using the semiclassical Marcus formalism,[17,18] as exemplified in a recent study of various discotic materials.[19]

$$k_{ET} = \frac{4\pi^2}{h} t^2 \frac{1}{\sqrt{4\pi\lambda RT}} e^{-\lambda/4RT} \qquad (1)$$

The rate of charge hopping depends primarily on two molecular parameters, λ and t (assuming that we operate in the low field limit and thus that there is no significant driving force induced by the applied electric field for the electron-transfer reaction). λ is the reorganization energy associated with the charge transfer process; it contains two contributions. The internal part reflects the amplitude of the geometric deformations of both molecules in going from the initial to the final redox state, while the external part describes the change in the nuclear and electronic polarization of the surrounding molecules. We will not discuss here the amplitude of the external reorganization energy because there are no simple means to evaluate it in the mesophase. This energetic contribution is, however, expected to be significant (a few tenths of an eV) and, in first approximation, rather insensitive to the exact chemical structure of the compounds under study because most of the organic conjugated materials are characterized by a similarly low dielectric constant. We have estimated the internal reorganization energy for the unsubstituted metal-free phthalocyanine molecule at the density functional theory (DFT) level using the B3LYP functional[20,21] and a 6-31g(d,p) basis set. This approach has been shown to provide theoretical estimates in very good agreement with experimental values deduced from gas-phase photoelectron spectra for several conjugated molecules.[22,23] We obtain values of 0.045 and 0.186 eV for the reorganization energy associated with the positive polarons (holes) and negative polarons (electrons), respectively. The alkoxy substitution leads to an increase in the reorganization energy (0.109 and 0.219 eV for holes and electrons, respectively), thus pointing to the role played by the nature of the anchoring units. The reorganization energy calculated for holes is smaller than that obtained for many other discotic molecules[19] and even for pentacene (for which a value around 0.1 eV is predicted at both the theoretical and experimental levels).[22] This should contribute to promoting fast hopping rates and, hence, a high mobility for the holes. This small value is rationalized by the fact that the geometry of the phthalocyanine is very similar in the ground state and in the singly positively charged state, see Figure 1. The changes in the bond lengths are more pronounced when going from the neutral molecule to the radical-anion and translate into a larger reorganization energy, which is detrimental for transport.

bond length	cation	anion
1	-65	+75
2	+79	-51
3	-51	+70
4	-10	+122
5	+12	-172
6	+2	+5
7	+33	+214
8	-31	-129
9	+58	+85
10	+8	+94
11	-59	-17
12	+77	-29
13	-68	-24
14	-24	-16

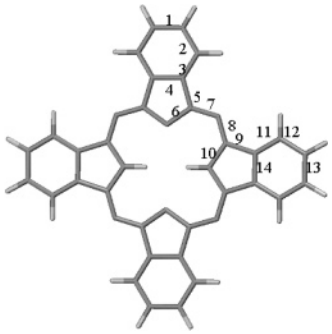

Figure 1. Changes (in 10^{-4} Å) in the bond lengths of the unsubstituted phthalocyanine molecule when going from the ground state to the radical-cation or radical-anion.

The second key parameter is the transfer integral, denoted t in eq 1, which describes the strength of the interactions and, hence, the ease of transferring the charge between adjacent molecules. We have estimated here the transfer integrals at the intermediate neglect of differential overlap (INDO)[24] level as half the splitting of the HOMO [LUMO] level for holes [electrons] in a dimer formed by two molecules in their ground-state geometry.[25,26] Because the electronic splittings are highly sensitive to the actual supramolecular organization within the columns,[25] we have analyzed the impact on the transfer integrals of the three main molecular motions expected in the discotic mesophases (i.e., fluctuations in the intermolecular distance, rotation of one molecule around the stacking axis, and translation of one disk occurring when mesogens are tilted in the columns); to do so, we have performed calculations on model stacks by considering as a starting point a configuration where the two disks are exactly superimposed on top of one another.

The electronic splittings decrease exponentially when the intermolecular distance is increased, as rationalized by the exponential decay of the p_z orbitals away from the nuclei. Short intermolecular distances are thus desirable to promote high hopping rates.

The rotation of one molecule around the stacking axis leads to pronounced fluctuations in the electronic splittings (Figure 2), in agreement with previous calculations based on the estimates of orbital overlaps.[27] Maxima are found every 45 degrees; they correspond to conformations where the overlap between the wave functions is optimal both for holes and

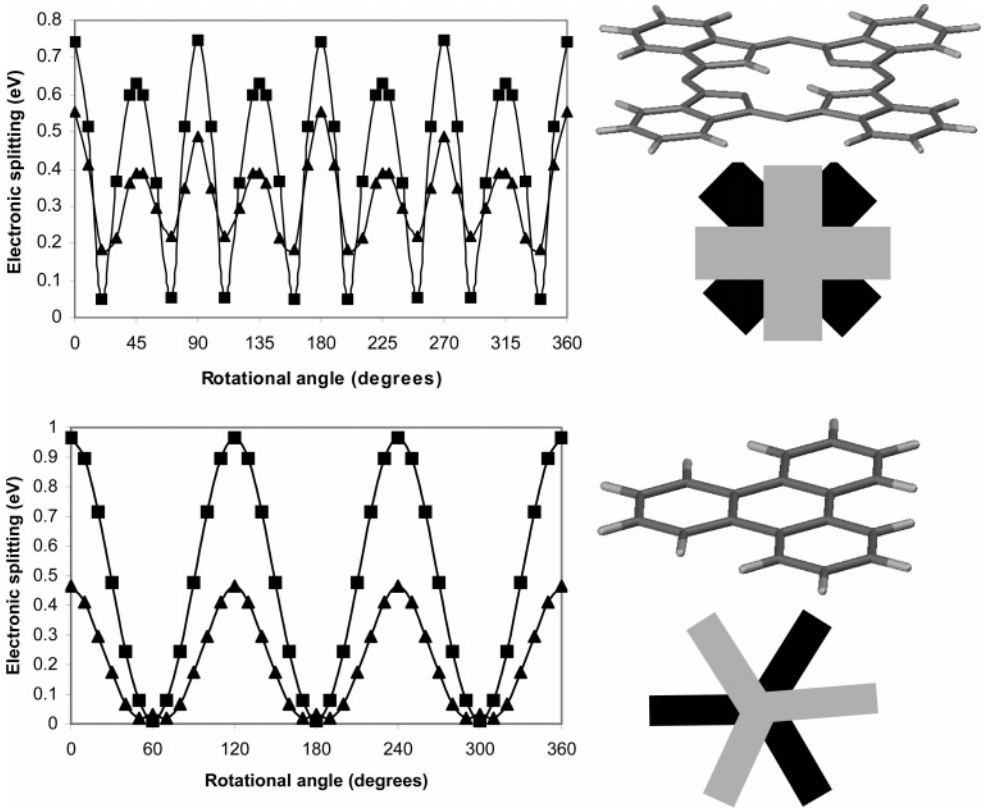

Figure 2. INDO-calculated electronic splittings (squares for the HOMO level and triangles for the LUMO level) in a dimer made of two phthalocyanine (up) and triphenylene (bottom) molecules when rotating one molecule around the stacking axis. The intermolecular distance is fixed at 3.5 Å. We also illustrate the molecular packing expected in nontilted columns for the two compounds.

electrons. Minima are found between (they are shifted by 22.5 degrees with respect to the maxima) and yield splittings that can reach values close to zero for holes. Interestingly, a local maximum is observed for a rotational angle of 45 degrees, which should prevail in nontilted columns in order to minimize the steric interactions between the peripheral chains.[28] This contrasts with triphenylene, for which the equilibrium angle, expected to be on the order of 60 degrees, lies around a minimum (Figure 2); this provides a strong hint to rationalize the small mobility values reported for triphenylene-based compared to phthalocyanine-based mesophases (~0.02 cm^2/Vs versus 0.2 cm^2/Vs).[29]

The lateral displacement of one molecule (reflecting the appearance of a tilt angle in the columns) generally has a dramatic impact on the electronic splittings, as illustrated in Figure 3 for a dimer made of two units rotated by 45 degrees. The decrease in the amplitude of the transfer integrals is driven by the fact that the overlap between the wave functions is reduced with the translation and finally drops to zero at large distances. The decay is not monotonic because a few secondary maxima are observed during the course of the translation for some specific conformations, promoting a good overlap between the wave functions. A tilt in the columns thus leads to a significant reduction in the transfer integrals, except if the translation accidentally leads to a tilt angle favoring high electronic splittings.

Energy Migration. We now turn to the characterization of energy transfer processes in phthalocyanine stacks. We have modeled here this process in first approximation as an excitation hopping between neighboring disks. Because the lowest excited state of phthalocyanine is strongly optically coupled to the ground state, the Förster mechanism based on the interaction of the transition dipole moments of the two interacting molecules[30] is expected to dominate over the Dexter mechanism,

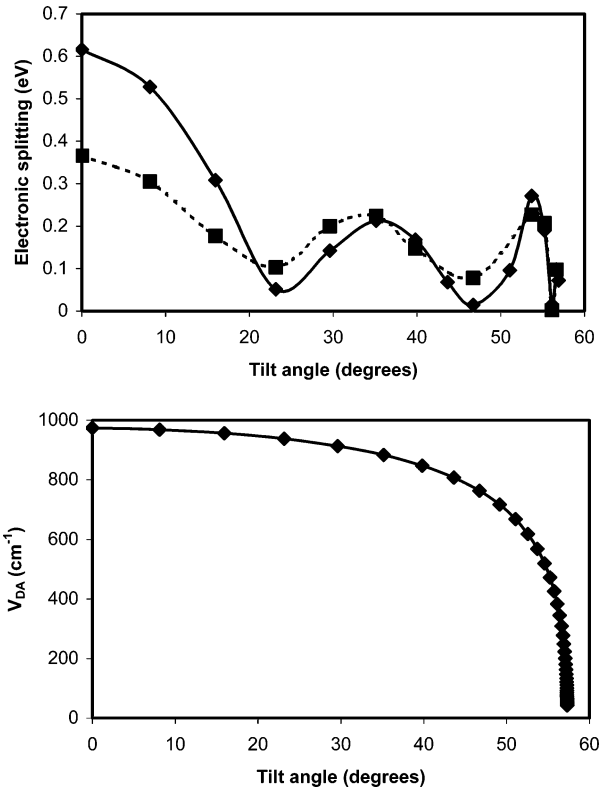

Figure 3. Top: Evolution of the electronic splittings (diamonds for the HOMO level and squares for the LUMO level) in a dimer made of two phthalocyanine molecules rotated by 45 degrees as a function of the tilt angle relative to the column axis. Bottom: The corresponding evolution for V_{DA11} is reported. The intermolecular distance is set at 3.5 Å in both cases.

which relies on the direct overlap between the HOMO and LUMO levels of the two units.

A Förster transfer can be viewed as the simultaneous deexcitation of a donor and excitation of an acceptor giving rise to the virtual exchange of a photon. The rate of exciton hopping, k_{EN}, is given (in ps^{-1}) by:[31]

$$k_{EN} = 1.18\,|V_{DA}|^2\,J_{DA} \qquad (2)$$

where J_{DA} is the overlap (expressed in cm) between the normalized emission spectrum of the donor and the normalized absorption spectrum of the acceptor; this term is weakly affected by changes in the supramolecular organization and has not been estimated in our study. V_{DA} is the electronic coupling (in cm^{-1}) between the donor and the acceptor playing the role of t in charge transport. This dipole−dipole interaction term has been calculated beyond the usual point−dipole approximation by expanding the transition dipoles into atomic contributions in order to account for the molecular topology of the Pc molecule:[32]

$$V_{DA} = \frac{1}{4\pi\epsilon_0}\sum_{m}^{D}\sum_{n}^{A}\frac{Q_D(m)Q_A(n)}{r_{mn}} \qquad (3)$$

where m and n run over all sites of the donor and acceptor, respectively; $Q_D(m)$ and $Q_A(n)$ are the atomic transition densities on sites m of the donor and n of the acceptor, separated by the distance r_{mn}. These values have been calculated with the INDO Hamiltonian coupled to a single configuration interaction (SCI) scheme. Because the phthalocyanine molecule has actually two low-lying excited states that are almost degenerate (they are separated by 0.08 eV according to the INDO/SCI calculations and by 0.09 eV in experimental absorption spectra recorded in solution, vide infra), both should contribute to the energy migration process. We have thus to consider four different pathways: from the first (second) excited state of molecule 1 to the first (second) excited state of molecule 2 (denoted as 11 (22)) and the cross-talks from the first (second) excited state of molecule 1 to the second (first) excited state of molecule 2 (denoted as 12 (21)). The actual dynamics of the energy transfer will be driven by both the relative initial population of the two states at a given temperature and the relative rates of the different pathways.

In a dimer made of two Pc molecules exactly superimposed and separated by 3.5 Å, V_{DA}^{22} is slightly larger than V_{DA}^{11} (1800 cm^{-1} vs 1460 cm^{-1}); these values are in good agreement with the numbers reported in the literature.[33] In contrast, V_{DA}^{12} and V_{DA}^{21} are negligible because the transition dipole moments of the lowest two excited states are orthogonal, being oriented along the two molecular branches of the phthalocyanine backbone. This situation is reversed when one molecule is rotated by 90 degrees, while all pathways become efficient for intermediate angles (Figure 4). We thus conclude that there is always an efficient pathway whatever the rotational angle; this also holds true for energy transfer processes at longer distances (i.e., between nonadjacent molecules) that are expected to occur along the stacks for a Förster mechanism. Similarly, the translation of one molecule impacts much less the electronic couplings than the transfer integrals, as illustrated for V_{DA}^{11} in Figure 3. The electronic coupling V_{DA} is, therefore, much less sensitive to rotational and translational disorder than transfer integrals.

In summary, we have demonstrated that charge and exciton transport in nontilted columns made of phthalocyanine molecules should be highly efficient in view of the large calculated

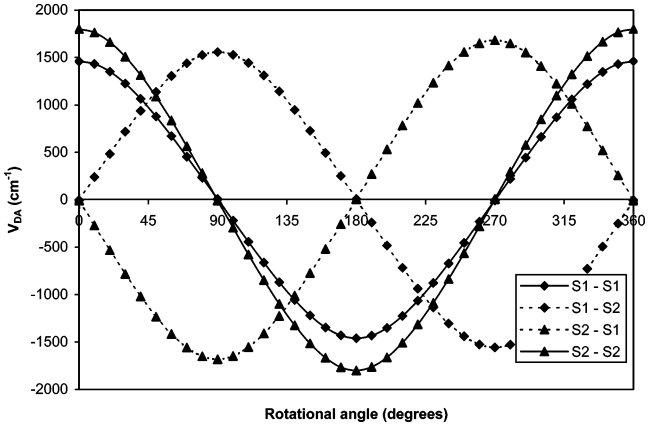

Figure 4. Evolution of V_{DA} as a function of the rotational angle for the different pathways in a dimer made of two phthalocyanine molecules separated by a distance of 3.5 Å.

electronic couplings. Such attractive properties are preserved upon introduction of a moderate tilt angle in the columns. The results further indicate that the dimensionality of the molecule represents a key parameter for energy transfer processes by introducing a degeneracy of the electronic levels and, in turn, a high insensitivity to rotational disorder. These theoretical results have thus triggered the synthesis, mesophase engineering, structural elucidation, and spectroscopic investigation of LC phthalocyanines **1a**,**b**, which are described in the following sections.

Molecular Design and Synthesis

LC Pcs bearing four substituents have many advantages over their 8-fold substituted analogues. The latter require three or four synthetic steps from commercially available reagents,[34] whereas the former are available within two synthetic steps.[35] Four-fold substituted Pcs can only be synthesized as a quasi-statistical mixture of the four isomers generated during the cyclotetramerization reaction.[16,36] It is anticipated that the presence of a mixture decreases the phase transition temperatures in comparison to the 8-fold substituted analogues. Moreover, the presence of four isomers of the 4-fold substituted LC Pcs prevents crystallization at low temperature.[3] Electronic structure calculations performed at the INDO level further indicate that the four isomers have their HOMO and LUMO levels at almost the same energy, thus preventing trapping effects for charge and exciton transport (see Supporting Information). The use of branched side chains also has a double advantage: (i) the presence of an asymmetric carbon atom in each alkyl chain creates a set of diastereoisomers; this large number of slightly structurally distinct molecules helps to prevent crystallization; and (ii) branching makes the chains more bulky; this destabilizes the packing of the microsegregated aliphatic parts of the mesogens by steric hindrance and decreases the clearing temperature.

The synthesis of Pcs **1a,b** has been performed in two steps, as depicted in Scheme 2. Nucleophilic substitution of the nitro group of the commercially available 4-nitrophthalonitrile **2** with the corresponding alcohol **3a,b** in dimethyl sulfoxide in the presence of lithium hydroxide has been performed by using a previously reported method, yielding 50−54% of **4a,b** after purification.[37] When **4a,b** are stored at room temperature (RT), the slightly yellow oils gradually turn to a slightly green color within a few days, thus pointing to uncontrolled Pcs formation. To avoid this process, **4a,b** were kept at −20 °C. The second step consists of the cyclotetramerisation of 4-alkoxyphthaloni-

TABLE 1: Thermotropic Properties of Mesogens 1a,b

compound	phase behavior	cell parameters (Å)	
H2Pc-O-(12,8)$_4$	Col_r 68 (0.05) Col_h 226 (3.2) I	Col_r at 27 °C:	Col_h at 160 °C:
1a	I 225 (−3.2) Col_h 68 (−0.08) Col_r	$a = 48.6$	$a = 30.4$
		$b = 30.6$	
H2Pc-O-(14,10)$_4$	Col_r 60 (0.05) Col_h 180 (3.3) I	Col_r at 27 °C:	Col_h at 160 °C:
1b	I 174 (−3.2) Col_h 57 (−0.05) Col_r	$a = 52.5$	$a = 31.8$
		$b = 32.1$	

The heating and cooling rates are set to 10 °C/min. All peak values are obtained from the second heating−cooling scan. Col_r = columnar rectangular mesophase; Col_h = columnar hexagonal mesophase; I = isotropic liquid. The transition temperatures are expressed in °C and ΔH in kJ/mol.

SCHEME 2: Two-Step Synthetic Pathway Leading to Mesogenic Phthalocyanines 1a,b[a]

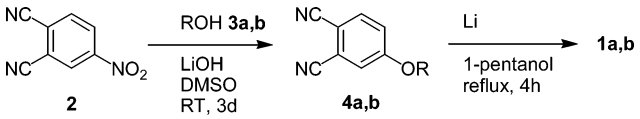

[a] **3a,b** are the alcohols corresponding to the alkyloxy side chains depicted in Scheme 1.

trile **4a,b** in the presence of metallic lithium in refluxing 1-pentanol.[38] **1a,b** are obtained as dark-green pasty materials, in yields ranging from 43 to 50% after purification by column chromatography. Compounds **1a,b** are soluble in organic solvents of various polarity such as tetrahydrofuran, methylene chloride, toluene, and hexane. The UV−vis, ^{1}H NMR, and MS spectral characteristics of Pcs **1a,b** are in agreement with their chemical structures. The metal-free character of the Pcs **1a,b** is confirmed: (i) by MS; (ii) by the presence of two intense absorption bands in the Q-band region (vide infra); and (iii) by the presence of a ^{1}H NMR signal around −2.8 ppm versus TMS. The three sets of signals observed in the aromatic region of the ^{1}H NMR spectra reveal the presence of a mixture of isomers.[36] The purity of the different materials has systematically been assessed by thin layer chromatography. Several grams of derivatives **1a,b** were readily obtained, allowing for the investigation of their physical properties.

Thermotropic Properties and Molecular Dynamics Simulation

Pcs **1a,b** exhibit two distinct LC phases going from RT to the isotropic melt, as evidenced by differential scanning calorimetry (DSC), cross-polarizing microscopy (CPM), and X-ray diffraction.

The calorimetric data obtained for compounds **1a,b** are collected in Table 1. A low-temperature transition occurs at 68 and 60 °C for **1a** and **1b**, respectively. The associated transition enthalpies (ΔH) amount 0.05 kJ/mol. Such low enthalpies are generally associated with transitions between phases of comparable structures.[39] The high-temperature transitions take place at 226 and 180 °C for **1a** and **1b**, respectively. The enthalpy values, on the order of 3.2−3.3 kJ/mol, are characteristic of clearing points (i.e., transitions from a mesophase to an isotropic liquid phase),[39] as confirmed by CPM (vide infra). Upon cooling, a small overcooling of 0−3 °C is observed for the different transitions.

Mesogens **1a,b** exhibit fluid and birefringent phases from RT to clearing temperature. Upon fast cooling from the isotropic melt, a pseudo focal-conic texture, typical of columnar hexagonal mesophases (Col_h), is observed below 226 and 180 °C for **1a** and **1b**, respectively.[40] At lower temperature, the optical texture evolves to a "fingerprint" texture, characteristic of columnar rectangular mesophases (Col_r).[41] This change occurs around the low-temperature transition observed by DSC at 68 and 60 °C for **1a** and **1b**, respectively. A homeotropic alignment is observed between two glass slides when cooling slowly **1b** from the isotropic melt to the Col_h mesophase, as evidenced by the presence of millimeter-wide nonbirefringent domains.[42] This regular alignment of the columnar axes perpendicular to the surface of the glass slides appears to be maintained at room temperature in the Col_r mesophase, as supported by the absence of birefringence. In view of the small tilt angle of the mesogens versus the columnar axis (vide infra), the latter phase remains structurally close to a Col_h mesophase, a feature of great interest for device applications. To the best of our knowledge, it is the first report of a columnar rectangular mesophase in which the columnar axes maintain a regular alignment upon cooling from a homeotropically aligned Col_h phase. The supramolecular organizations of **1a,b** have been studied by temperature-dependent X-ray diffraction on nonoriented samples (powder samples). The cell parameters are given in Table 1, and the detailed X-ray data are collected in the Supporting Information. The high-temperature mesophases of **1a,b** present, at small angles, a pattern of reflections for which reciprocal spacing follows the ratio $1:\sqrt{3}:\sqrt{4}:\sqrt{7}$. They can be indexed as the 10, 11, 20, and 21 reflections of two-dimensional (2D) hexagonal lattices. In the wide-angle region, the presence of a halo between 4.6 and 5.1 Å can be associated with the average distance of the liquidlike side chains.[43] A shoulder appears at larger angles, pointing to an average stacking distance along the column of about 4.0 Å. The broad diffuse intensity shows that mesogens are weakly ordered along the columns.[44] At low temperatures (below 68 and 60 °C for **1a,b**, respectively), the diffraction patterns of both compounds are consistent with a columnar rectangular mesophase (Col_r). The extinction of all the reflections with $h + k \neq 2n$ allows us to assign the *c*2*mm* symmetry to the rectangular 2D lattices. Besides the halo corresponding to the liquidlike alkyl chains, a shoulder is observed at wide angles and suggests an average $\pi-\pi$ stacking distance of about 3.5 Å in the columns. On the basis of the X-ray data, the density is estimated to be ∼1.1 g/cm^3 for both compounds at room temperature. It should be stressed that these values are crude estimates because the shoulders from which the $\pi-\pi$ stacking distances are deduced are very diffuse and overlaid by the halo of the alkyl chains.

The cell parameters indicate that the high-temperature Col_h and low-temperature Col_r mesophases exhibit only slightly different intercolumnar distances. This structural observation corroborates the rather low transition enthalpies between these two phases. The disk diameters estimated at the molecular dynamics level (based on the Dreiding force field) with an explicit account of the side chains in their most probable conformation is ∼46 and ∼48 Å for **1a** and **1b**, respectively. These values are significantly larger than the experimental diameter inferred for **1a** (30.4 Å) and for **1b** (31.8 Å), which points to the interdigitation of the alkyl side chains and their

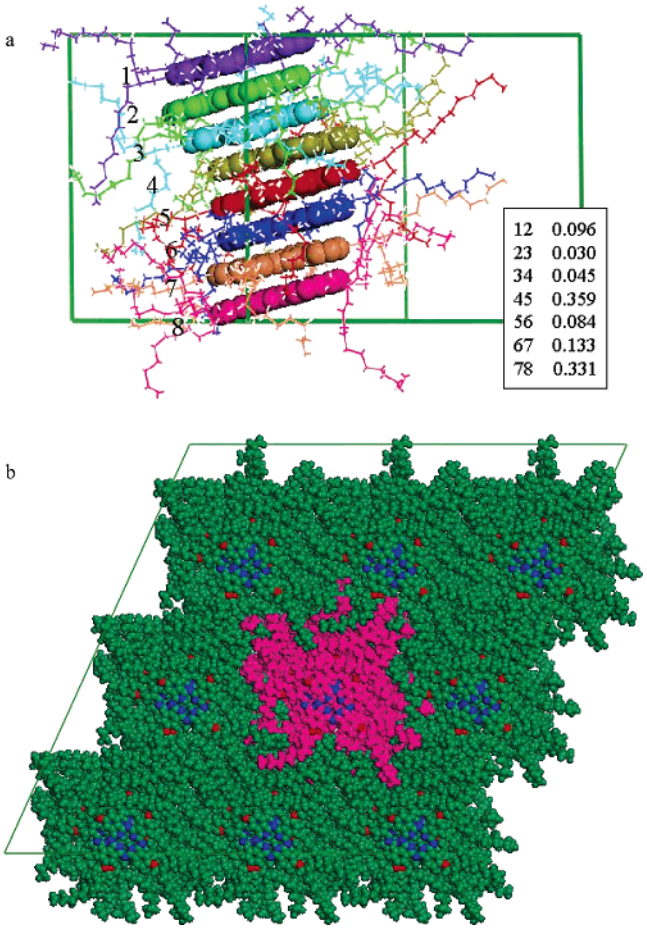

Figure 5. (a) Snapshot of a molecular dynamics simulation of **1b** in its rectangular phase. The HOMO splittings (in eV) between adjacent molecules are also reported on the basis of the numbering given in the snapshot. (b) Top view of a supercell made of 3 × 3 unit cells containing 8 stacked molecules, as generated by the molecular dynamic simulations.

deviation from the plane of the flat aromatic phthalocyanine cores.

The supramolecular organization deduced from the X-ray data for the rectangular phase of compound **1b** is further supported by molecular dynamics simulations. The procedure adopted to obtain the results is provided in the Experimental Section. A snapshot from a simulation of 4.5 ns performed at 300 K is shown in Figure 5a. The calculated average distance between the disks is 3.5 Å and the tilt angle between the planes of the Pc cores and the axis of the column is calculated to be 16°, in excellent agreement with the experimental value of 15° obtained by 2D X-ray diffraction on oriented fibers.[45] The centers of the Pc cores are not all located on the columnar axis, as can clearly be seen in Figure 5a; this arises from changes in the lateral shifts between adjacent molecules along the column. The rotational angle between two neighboring molecules also varies along the stack in a range from 20° to 40°. Figure 5a further illustrates that, while the Pc cores are regularly packed, the alkyl chains are highly disordered. Most of them do not remain in the plane of the molecule to which they are connected; they are actually strongly twisted upward or downward and mix with the alkyl chains of the adjacent molecules. To better visualize the interpenetration of the lateral alkyl chains belonging to adjacent columns, a supercell made of 9 (3 × 3) unit cells is displayed in Figure 5b. The atoms of the molecules in the central column are displayed in pink, while those located in the eight adjacent columns are displayed in green (except for the nitrogen

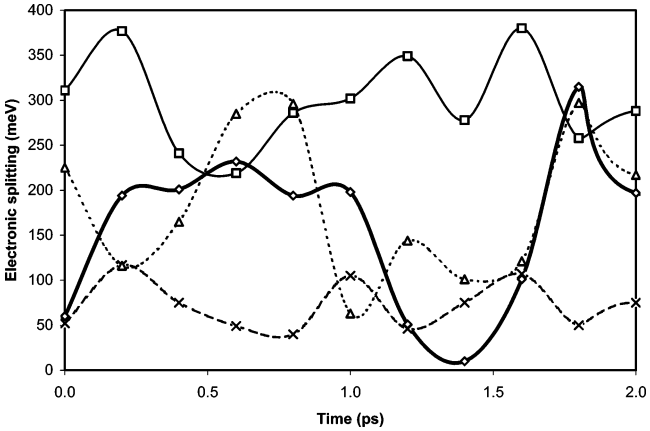

Figure 6. Time evolution of the INDO-calculated HOMO splittings as a function of the geometric fluctuations in the stacks provided by the molecular dynamics simulations. The evolution is reported here for a time lapse of 2 ps for four dimers extracted from the model stack (squares for 45; triangles for 67; diamonds for 23; crosses for 12).

and oxygen atoms which appear in blue and red, respectively). This picture illustrates that the columns are not strictly delimited laterally in view of the strong interpenetration of the alkyl coronae. It is easy to visualize from Figure 5 that the alkyl side chains are in a liquidlike state and that they significantly deviate from the plane of the rigid phthalocyanine cores. The shortest two distances calculated between neighboring stacks, 32.3 and 35.6 Å, are in good agreement with the experimental value of 30.8 and 32.1 Å obtained for **1b** in its Col_r phase.

We also report in Figure 5a the calculated HOMO splitting between adjacent molecules in the simulated stack; they are found to vary significantly (from 0.03 to 0.36 eV) depending on the amplitude of the rotational angle and of the lateral shift.[46] The splittings also incorporate a contribution arising from the fact that the HOMO of the two molecules are different before interacting because of their different molecular environments; this effect could thus promote an apparent splitting of the electronic levels for situations where the effective transfer integrals are close to zero. The fact that splittings as small as 0.03 eV are calculated indicate that this effect is, however, negligible. The conformations promoting the weakest transfer integrals will thus limit the hole mobility values that will be driven by a subtle interplay between the relative rate and relative weight associated with the various dimer configurations.

We have reported in Figure 6 the evolution of the INDO-calculated HOMO splittings for four dimers extracted from the stack over a period of time of 2 ps; the fast variations observed for some splittings demonstrate the occurrence of fast geometric fluctuations in the columns. Thus, the charges are not drifting through a frozen system, and the interplay between charge transfer rates and geometry fluctuation dynamics must be accounted for to provide a full picture of charge transport in these systems. The results further indicate that conformational gating is operative, in other words, that the system can modify its conformation very fast and thus quickly depart from structures limiting the charge transport.

Photophysical Properties in Solid State

Phthalocyanines are well-known for their intense light absorption in the visible part of the solar spectrum, which yields deep-blue to dark-green materials depending on the nature of the peripheral groups and on the presence or absence of a metallic atom inside the cavity of the aromatic core.[3] A single broad absorption band is observed for **1b** at long wavelength,

with a maximum intensity at 615 nm in solid state (see Supporting Information). The blue-shift (92 nm) observed when going from solution (maximum at 707 nm) to the solid state is characteristic of the formation of H-aggregates[47] and confirms the stacking of the molecules in the columns. This is further supported by the quenching of the luminescence in the solid state.[48] The peak at 334 nm is less affected by aggregation than the Q-band. The absorption spectrum of **1b** reversibly changes upon heating from room temperature to 145 °C and subsequent cooling to room temperature, even at the Col_r-Col_h transition. The absorption maximum shifts to the red from 611 nm at 25 °C to 616 nm at 145 °C and is accompanied by a decrease in absorption intensity (hypochromic shift). No noticeable change occurs at the Col_h-Col_r transition, although the disks stack perpendicular to the column axis in the hexagonal mesophase and are tilted in the rectangular mesophase. The absence of singularity in the evolution of the absorption spectra at the phase transition further confirms that the difference in the molecular packing between the two mesophases is weak; this is consistent with the existence of a small tilt angle in the Col_r phase, which should not hamper drastically charge transport in the columns.

To estimate the absorption coefficient α of **1b** in the solid state, the thickness and absorption at 615 nm of six spin-coated films have been measured by using atomic force microscopy (AFM) and UV−vis spectroscopy, respectively. A value of $4.2 \times 10^4 \pm 0.3 \times 10^4$ cm^{-1} has been calculated for the solid-state absorption coefficient at 605 nm from:

$$\alpha = -\ln(10^{-A})/d \qquad (4)$$

where A is the absorbance and d the thickness of the film. Other materials commonly used in solar cells present higher absorption coefficients: 2.5, 1.9, 1.9, and 1.8×10^5 cm^{-1} for zinc phthalocyanine, 1-(3-methoxycarbonyl)propyl-1-phenyl-[6,6]-methanofullerene (PCBM), poly[2-methoxy-5-(3′,7′-dimethyl-octyloxy)-1,4-phenylene vinylene] (MDMO-PPV) and poly(3-hexylthiohene-2,5diyl) (P3HT), respectively.[49] This can be explained by the presence of long alkyl chains in our compounds that dilute the aromatic cores and thereby reduce the density of absorbing moieties.

Conclusions

It is concluded from theoretical results that metal-free LC phthalocyanines have a great potential as charge and exciton carriers. According to quantum calculations performed on model systems, hole transport is favored in phthalocyanines by a low reorganization energy and by large electronic splittings for rotational angles between disks around 45° that should correspond to the preferential conformations within columnar stacks. However, a large distribution of electronic splittings is obtained from structures derived from molecular dynamics simulations as a result of the inherent structural disorder in LC phases; interestingly, these simulations also suggest that the geometry of the stacks fluctuates very fast, thus allowing for conformational gating. In contrast, energy transfer is rather insensitive to structural disorder due to the two-dimensional character of the Pc core, which creates the conditions for an efficient pathway, with or without a small tilt angle in the columns, whatever the rotational angle between adjacent disks. The promising charge and exciton transport properties coupled to the well-documented intense long-wavelength absorption, thermal inertness, and nontoxicity of phthalocyanines qualify them as attractive materials to be used in organic photovoltaic cells.

These theoretical results have motivated the design, synthesis, and characterization of liquid crystalline phthalocyanines with a set of tailored properties, i.e. with a synthetic availability on the gram scale, a high solubility for solution processing, a columnar mesophase that persists down to RT, and a clearing temperature below 200 °C to allow for a homeotropic alignment. Future work will be devoted to measuring the charge and exciton transport properties of these materials and to incorporating them in solar cells.

Experimental Section

General. ^{1}H NMR and ^{13}C NMR spectra were recorded in DMSO-d_6 and C_6D_6 on a Bruker Advance 300 with solvent signal as the internal standard. Mass spectra were recorded on a VG Micromass 7070F instrument (electron impact, 70 eV) and a VG analytical ZAB 2-SE-FPD:FD (8 kV). UV−Vis absorption measurements were carried out in solution with a HP 8453 spectrophotometer and in the solid state with a Perkin-Elmer Lambda 5 spectrophotometer. The emission measurements were carried out with a SLM-Aminco 3000 diode array spectrophotometer. Thin solid films have been obtained by spin-coating, with a Chemat Tech. spin-coater KW-4A, from chloroform solutions of the corresponding compounds onto quartz or glass slides. Thin layer chromatography (TLC) has been performed on Silicagel 60 T_{254}.

The thermal behavior of all the synthesized materials was investigated by polarizing optical microscopy (JENA microscope equipped with a Mettler FP 52 hot stage) and differential scanning calorimetry (Mettler Toledo DSC 821, 2−6 mg samples in closed Al pans) with heating and cooling scans performed at 10 °C/min (peak values are given). Powder X-ray diffraction investigations were carried out using a Siemens D 500 Kristalloflex with a graphite-monochromatized Cu Kα X-ray beam emitted from a Rotating Rigaku RV-300 anode. The temperature of the sample on a copper sample holder was monitored with a bimetal sensor, previously calibrated by reference measurements. All the reagents were purchased from Aldrich and used as received. DMSO (A.C.S. reagent, Aldrich) was refluxed over CaO and distilled under vacuum freshly before use. 1-Pentanol (A.C.S. reagent, Aldrich) was refluxed over magnesium 1-pentanolate and distilled freshly before use. The solvents for the photophysical study were of spectroscopic grade and used as received. Column chromatographies were performed on silica gel (Merck silica gel 60, mesh size 0.2−0.5 mm).

General Procedure for the Synthesis of 4a,b. A mixture of 4-nitrophthalonitrile **2** (4.50 g, 26 mmol) and the appropriate alcohol (39 mmol) in 100 mL anhydrous methylsulfoxide was stirred for 2 h at RT. Lithium hydroxide powder (1.25 g, 52 mmol) was then added under stirring. The reaction medium turned from yellow to black and was stirred for 3 days at RT. The solution was poured in water and extracted three times with ethyl acetate. The combined organic fractions were dried on Na_2SO_4, filtered, and evaporated. The crude products (a dark green-yellow oil) were purified on a silica gel column chromatography with toluene as eluent to afford the pure 4-alkoxyphthalonitrile **4a** and **4b** as a viscous light-yellow oil, with yields of 50 and 57%, respectively. Compounds **4a,b** were stored at −20 °C to avoid uncontrolled cyclotetramerization.

4-(2-Octyldodecyloxy)-phthalonitrile (4a). Yield 57%. ^{1}H NMR ($CDCl_3$): δ (ppm) 0.88 (m, 6H), 1.2−1.5 (m, 32H), 1.81 (m, 1H), 3.93 (d, $J = 5.5$ Hz, 2H), 7.19 (dd, $J = 8.8$ and 2.6 Hz, 1H), 7.27 (d, $J = 2.6$ Hz, 1H), 7.71 (d, $J = 8.8$ Hz, 1H). MS (EI) $m/z = 424$ (M^+), 281, 183, 169, 155. R_F (silica gel, toluene): 0.55.

4-(2-Decyltetradecyloxy)-phthalonitrile (4b). Yield 50%. ^{1}H NMR ($CDCl_3$): δ (ppm) 0.88 (t, J = 6.6 Hz, 6H), 1.2 (br m, 40H), 1.81 (m, 1H), 3.91 (d, J = 5.6 Hz, 2H), 7.17 (dd, J = 8.7 and 2.4 Hz, 1H), 7.25 (d, J = 2.2 Hz, 1H), 7.69 (d, J = 8.7 Hz, 1H). ^{13}C NMR (C_6D_6): δ (ppm) 162.0, 134.8, 119.3, 118.8, 117.66, 116.0, 115.7, 107.5, 71.7, 38.1, 32.3, 31.5, 30.4, 30.2, 30.2, 30.1, 29.8, 27.2, 23.1, 14.4. MS (EI) m/z = 480 (M^+), 337, 155, 141, 127, 113, 99, 85, 71, 57. R_F (silica gel, toluene): 0.55.

General Procedure for the Synthesis of 1a,b. 4-Alkoxyphthalonitrile **4** (1 g) was mixed with a large excess of metallic lithium, in 6 mL of dry 1-pentanol. The reaction mixture was then heated to reflux under an argon atmosphere. After 4 h, 30 mL of acetic acid were added to the dark-green solution. The precipitate was collected by filtration and washed with water and methanol. The pasty-green material obtained was then dissolved in methylene chloride, and the solvent was evaporated under vacuum. The pure product was obtained after purification on silica gel column chromatography (toluene/hexane 1:1 as eluent) to afford 43 and 50% of **1a** of **1b**, respectively.

2,9(10),16(17),23(24)-Tetra(2-octyldodecyloxy)-phthalocyanine (1a). Yield 43%. ^{1}H NMR (C_6D_6): δ (ppm) −3.24 (br, 2H), 0.94 (t, J = 6.5 Hz, 12H), 1.00 (t, J = 6.8 Hz, 12H), 1.3−2.0 (m, 112H), 2.1 (br, 2H), 2.2 (br, 2H), 4.08 (br, 4H), 4.30 (br, 4H), 7.51−7.75 (m, 4H), 8.49−8.69 (m, 4H), 8.97−9.17 (m, 4H). MS (FD) m/z = 1700 (M^+), 2268 ($4M^+/3$), 2551 ($3M^+/2$), 2836 ($5M^+/3$), 3402 ($2M^+$). UV−vis (toluene): λ_{max} (ϵ) = 705 nm (132 000 ± 13 000 L·mol^{-1}·cm^{-1}), λ (ϵ) = 671 nm (127 000 ± 13 000 L·mol^{-1}·cm^{-1}), λ (ϵ) = 344 nm (114 000 ± 13 000 L·mol^{-1}·cm^{-1}).

2,9(10),16(17),23(24)-Tetra(2-decyltetradecyloxy)-phthalocyanine (1b). Yield 50%. ^{1}H NMR (C_6D_6): δ (ppm) −3.1 (br, 2H), 0.91 (m, 24H), 1.3−2.0 (m, 120H), 2.1 (br, 2H), 2.2 (br, 2H), 4.10 (br, 4H), 4.32 (br, 4H), 7.55−7.76 (m, 4H), 8.56−8.73 (m, 4H), 9.01−9.20 (m, 4H). MS (FD) m/z = 962 ($M^+/2$), 1924 (M^+), 2564 ($4M^+/3$), 2886 ($3M^+/2$), 3207 ($5M^+/3$), 3366 ($7M^+/4$). UV−vis (toluene): λ_{max} (ϵ) = 705 nm (149 000 ± 15 000 L·mol^{-1}·cm^{-1}), λ (ϵ) = 671 nm (146 000 ± 15 000 L·mol^{-1}·cm^{-1}), λ (ϵ) = 344 nm (129 000 ± 15 000 L·mol^{-1}·cm^{-1}).

Theoretical Methodology. An UFF-like force field (based on the Dreiding force field[50] was used for all simulations without electrostatic contributions. Owing to its similarities with the UFF potential,[51] the Dreiding potential functions were used as a framework to impose constraints to the torsion angles around all CC and NC bonds involved in the conjugation in order to maintain the conjugated cores planar.

The initial configuration of the system consists of a stack of 8 molecules in a monoclinic cell (parameters $a = b$ = 60 Å, c = 32 Å, $\alpha = \beta = 90°$, $\gamma = 63°$), each molecule being rotated by 45° with respect to its neighbors. After an initial minimization procedure, we performed a NVT molecular dynamics (MD) simulation during 50 ps and then a NPT dynamics under an external pressure of 0.5 GPa during 50 ps. The final parameters a and b are 38 and 35 Å, respectively. At this stage, we changed the value of the parameter a to 35 Å and minimized again the structure. An annealing cycle was next run from 1000 K toward 300 K over a period of 170 ps. It was followed by a NPT dynamics at 1 atm during 50 ps; the resulting parameters a and b are then found to be 34 and 33 Å, respectively. Parameter a was changed to 33 Å, and the structure was minimized once again. We performed another annealing cycle of 170 ps at 1500 K followed by NPT simulations extending up to 4.5 ns in order to achieve equilibration. The final parameters of the system are a = 32.1 Å, b = 32.6 Å, c = 27.8 Å, $\alpha = 91°$, $\beta = 89°$, and $\gamma = 66°$. The density obtained from the simulations is slightly lower than the experimental value: 0.97 vs 1.07 g·cm^{-3}, respectively. However, because the error on the determination of the experimental density can be as large as 0.05 g·cm^{-3}, the value derived from the simulations can be considered as a good approximation of the experimental density. All calculations were performed by using the Cerius2 simulation package.[52]

Acknowledgment. This work has been financially supported by the Belgian National Science Foundation (FNRS FRFC no. 2.4560.00 and no. 2.4608.04), by the Communauté Française de Belgique (ARC no. 00/05-257), by the European Commission (FP5-DISCEL G5RD-CT-2000-00321, FP6-NAIMO integrated project NMP4-CT-2004-500355), by the Belgian Federal Science Policy Office (PAT SOLTEX and PAI 5-3), and by the Walloon Region (SOLPLAST). J.C., D.B., and E.H. are FNRS research fellows. J.T. and V.L. acknowledge the FRIA for doctoral fellowships. The help of Dr. Michel Luhmer for NMR experiments is greatly acknowledged.

Supporting Information Available: Structural isomers of **1b** and frontier orbital energies calculated at the INDO level. ^{1}H NMR spectrum of **1b** in $CDCl_2$-$CDCl_2$ at 100 °C. ^{1}H NMR spectrum of **1b** in C_6D_6 at 25 °C. ^{13}C NMR spectrum of **1b** in C_6D_6 at 25 °C. Cross-polarized microscope pictures of **1b**. X-ray diffraction peak assignment. Solution absorption and emission of **1b**. Absorption of **1b** upon concentration increase. Details of solid-state absorption coefficient calculation. This material is available free of charge via the Internet at http://pubs.acs.org.

References and Notes

(1) Braun, A.; Tcherniac, J. *Ber. Dtsch. Chem. Ges.* **1907**, *40*, 2709−2714.
(2) Herbst, W.; Hunger, K. In *Industrial Organic Pigments: Production, Properties, Applications*; Wiley-VCH: Weinheim, Germany, 1997.
(3) McKeown, N. B. In *Phthalocyanine Materials*; Cambridge University Press: Cambridge, U.K., 1998.
(4) Simon, J.; André, J.-J. In *Molecular Semiconductors: Photoelectrical Properties and Solar Cells*; Springer-Verlag: Berlin, 1985.
(5) Wang, M.; Chen, H. Z.; Yang, S. L. *J. Photochem. Photobiol., A* **1990**, *53*, 437−441.
(6) Piechocki, C.; Simon, J. *J. Am. Chem. Soc.* **1982**, *104*, 5245−5247.
(7) (a) Hanack, M.; Lang, M. *Adv. Mater.* **1994**, *5*, 819−833. (b) van Nostrum, C. F.; Nolte, R. J. M. *Chem. Commun.* **1996**, 2385−2392.
(8) Hatsusaka, K.; Ohta, K.; Yamamoto, I.; Shirai, H. *J. Mater. Chem.* **2001**, *11*, 423−433.
(9) Warman, J. M.; van de Craats, A. M. *Mol. Cryst. Liq. Cryst.* **2003**, *396*, 41−72.
(10) Blanzat, B.; Barthou, C.; Tercier, N.; André, J.-J.; Simon, J. *J. Am. Chem. Soc.* **1987**, *109*, 6193−6194.
(11) Orti, E.; Brédas, J. L.; Clarisse, C. *J. Chem. Phys.* **1990**, *92*, 1228−1235.
(12) Schmidt-Mende, L.; Fechtenkötter, A.; Müllen, K.; Moons, E.; Friend, R. H.; MacKenzie, J. D. *Science* **2001**, *293*, 1119−1122.
(13) MacDonald, W. A. *J. Mater. Chem.* **2004**, *14*, 4−10.
(14) Méry, S.; Haristoy, D.; Nicoud, J.-F.; Guillon, D.; Diele, S.; Monobe, H.; Shimizu, Y. *J. Mater. Chem.* **2002**, *12*, 37−41.
(15) (a) Schouten, P. G.; Van der Pol, J. F.; Zwikker, J. W.; Drenth, W.; Picken, S. J. *Mol. Cryst. Liq. Cryst.* **1991**, *195*, 291−305. (b) McKeown, N. B.; Painter, J. *J. Mater. Chem.* **1994**, *4*, 1153−1156. (c) Brewis, M.; Clarkson, G. J.; Helliwell, M.; Holder, A. M.; McKeown, N. B. *Chem.−Eur. J.* **2000**, *6*, 4630−4636.
(16) Rager, C.; Schmid, G.; Hanack, M. *Chem.−Eur. J.* **1999**, *5*, 280−288.
(17) Marcus, R. A. *Rev. Mod. Phys.* **1993**, *65*, 599−610.
(18) Barbara, P. F.; Meyer, T. J.; Ratner, M. A. *J. Phys. Chem.* **1996**, *100*, 13148−13168.
(19) Lemaur, V.; da Silva Filho, D. A.; Coropceanu, V.; Lehmann, M.; Geerts, Y.; Piris, J.; Debije, M. G.; van de Craats, A. M.; Senthilkumar, K.; Siebbeles, L. D. A.; Warman, J. M.; Brédas, J. L.; Cornil, J. *J. Am. Chem. Soc.* **2004**, *126*, 3271−3279.
(20) Becke, A. D. *J. Chem. Phys.* **1993**, *98*, 1372−1377.
(21) Lee, C.; Yang, W.; Parr, R. G. *Phys. Rev. B* **1988**, *37*, 785−789.

(22) Amashukeli, X.; Winkler, J. R.; Gray, H. B.; Gruhn, N. E.; Lichtenberger, D. L. *J. Phys. Chem. A* **2002**, *106*, 7593−7598.
(23) Gruhn, N. E.; da Silva Filho, D. A.; Bill, T. G.; Malagoli, M.; Coropceanu, V.; Kahn, A.; Brédas, J. L. *J. Am. Chem. Soc.* **2002**, *124*, 7918−7919.
(24) Zerner, M. C.; Loew, G. H.; Kichner, R. F.; Mueller-Westerhoff, U. T. *J. Am. Chem. Soc.* **1980**, *102*, 589−599.
(25) Brédas, J. L.; Beljonne, D.; Coropceanu, V.; Cornil, J. *Chem. Rev.* **2004**, *104*, 4971−5003.
(26) Cornil, J.; Lemaur, V.; Calbert, J. P.; Brédas, J. L. *Adv. Mater.* **2002**, *14*, 726−729.
(27) Pietro, W. J.; Marks, T. J.; Ratner, M. A. *J. Am. Chem. Soc.* **1985**, *107*, 5837−5852. Binstead, R. A.; Reimers, J. R.; Hush, N. S. *Chem. Phys. Lett.* **2003**, *378*, 654−659.
(28) Weber, P.; Guillon, D.; Skoulios, A. *Liq. Cryst.* **1991**, *9*, 369−382.
(29) van de Craats, A. M. Charge Transport in Self-Assembling Discotic Liquid Crystalline Materials. Ph.D. Thesis, Delft University of Technology, **2000**.
(30) Förster, T. *J. Chem. Soc., Discuss. Faraday Soc.* **1959**, *27*, 7−12.
(31) May, V.; Kühn, O. *Charge and Energy Transfer Dynamics in Molecular Systems*; Wiley-VCH: Weinheim, Germany, 2000.
(32) Beljonne, D.; Cornil, J.; Silbey, R.; Millié, P.; Brédas, J. L. *J. Chem. Phys.* **2000**, *112*, 4749−4758.
(33) (a) Orti, E.; Brédas, J. L.; Clarisse, G. *J. Chem. Phys.* **1990**, *92*, 1228−1235. (b) Oddos-Marcel, L.; Madeore, F.; Bock, A.; Neher, D.; Ferencz, A.; Rengel, H.; Wegner, G.; Kryschi, C.; Trommsdorff, H. P. *J. Phys. Chem.* **1996**, *100*, 11850−11856.
(34) Simon, J.; Bassoul, P. Phthalocyanine Based Liquid Crystals: Towards Submicronic Devices. In *Phthalocyanines: Properties and Applications*; Leznoff, C. C., Lever, A. B. P, Eds.; VCH: Weinheim, Germany, 1989.
(35) Clarkson, G. J.; Hassan, B. M.; Maloney, D. R.; McKeown, N. B. *Macromolecules* **1996**, *29*, 1854−1856.
(36) Görlach, B.; Dachtler, M.; Glaser, T.; Albert, K.; Hanack, M. *Chem.−Eur. J.* **2001**, *7*, 2459−2465.
(37) Young, J. G.; Onyebuagu, W. *J. Org. Chem.* **1990**, *55*, 2155−2159.
(38) Clarkson, G. J.; McKeown, N. B.; Treacher, K. E. *J. Chem. Soc., Perkin Trans. 1* **1995**, 1817−1823.
(39) Collings, P. J.; Hird, M. In *Introduction to Liquid Crystals: Chemistry and Physics*; Taylor & Francis: London, U.K., 1997.
(40) Barberá, J.; Rakitin, O. A.; Blanca Ros, M.; Torroba, T. *Angew. Chem., Int. Ed.* **1998**, *37*, 296−299.
(41) Suarez, M.; Lehn, J.-M.; Zimmerman, S. C.; Skoulios, A.; Heinrich, B. *J. Am. Chem. Soc.* **1998**, *120*, 9526−9532.
(42) van der Pol, J. F.; Neeleman, E.; Zwikker, J. W.; Nolte, R. J. M.; Drenth, W.; Aerts, J.; Visser, R.; Picken, S. J. *Liq. Cryst.* **1989**, *6*, 557−592.
(43) Levelut, A. M. *J. Chim. Phys.* **1983**, *80*, 149−161.
(44) Sleven, J.; Cardinaels, T.; Binnemans, K.; Nelis, D.; Mullens, J.; Hinz-Huebner, D.; Meyer, G. *Liq. Cryst.* **2003**, *30*, 143−148.
(45) Ivanov, D. A. Personal communication.
(46) Because force fields generally fail in describing the correct geometry of conjugated backbones, we have also calculated the splittings when imposing to the phthalocyanine core the geometry optimized at the DFT level; similar numbers are obtained in both cases.
(47) Ban, K.; Nishizawa, K.; Ohta, K.; Shirai, H. *J. Mater. Chem.* **2000**, *10*, 1083−1090.
(48) Cornil, J.; dos Santos, D. A.; Crispin, X.; Silbey, R.; Brédas, J. L. *J. Am. Chem. Soc.* **1998**, *120*, 1289−1299.
(49) Hoppe, H.; Sariciftci, N. S. *J. Mater. Res.* **2004**, *19*, 1924−1945.
(50) Mayo, S. L.; Olafson, B. D.; Goddard, W. A. *J. Phys. Chem.* **1990**, *94*, 8897−8909.
(51) Rappe, A. K.; Casewit, C. J.; Colwell, K. S.; Goddard, W. A.; Skiff, W. M. *J. Am. Chem. Soc.* **1992**, *114*, 10024−10035.
(52) Accelrys, formerly Molecular Simulations Inc., 9685 Scranton Road, San Diego, CA., 1997.